Synthesis of flower-like WO_3/Bi_2WO_6 heterojunction and enhanced photocatalytic degradation for Rhodamine B

Zhenfeng Zhu, Ying Yan, Junqi Li

School of Materials Science and Engineering, Shaanxi University of Science and Technology, Xi'an 710021, People's Republic of China
E-mail: zhuzf@sust.edu.cn

Published in Micro & Nano Letters; Received on 16th April 2015; Revised on 21st June 2015; Accepted on 7th July 2015

Flower-like Bi_2WO_6 microspheres were prepared by a facile hydrothermal process without any surfactant or template. The WO_3/Bi_2WO_6 samples were prepared by a simple heat treatment. The obtained samples were characterised by X-ray diffraction, field emission scanning electron microscopy, photoluminescence spectra, transient photocurrent and UV–vis absorption spectroscopy. In the heterojunctions, WO_3 nanoparticles adhered to the surface of the three-dimensional flower-like hierarchical Bi_2WO_6. The WO_3/Bi_2WO_6 samples showed much higher photocatalytic activity than pure Bi_2WO_6 did for Rhodamine B degradation under visible light irradiation. The improved photocatalytic activity is ascribed to the synergic effect between WO_3 and Bi_2WO_6 in the framework, which led to the high transfer rate of photoinduced charge carriers. The possible photocatalytic mechanism of the composites is proposed to further understand the improvement in photocatalytic activity.

1. Introduction: Semiconductor photocatalysis has been considered as a promising technology for the degradation of pollutants [1–3]. The semiconductor TiO_2 is considered as one of the most useful and valuable photocatalysts [4, 5]. However, the light response range of TiO_2 is limited to ultraviolet due to the wide bandgap (3.2 eV) [6], which accounts for only about 4% of natural sunlight [7–10]. So it is significant to prepare highly efficient visible-light photocatalysts, since visible light accounts for about 46% of entire sunlight.

Fortunately, Bi_2WO_6 has been demonstrated as one of the best visible-light-driven photocatalysts and has attracted great research interest because of its excellent photocatalytic property in wastewater purification [11–13]. Previous studies demonstrate that the flower-like Bi_2WO_6 structures exhibit good photocatalytic activity, because three-dimensional (3D) flower-like structures possess a large specific surface area which can improve the photoenergy conversion efficiency [2, 14]. Despite the flower-like Bi_2WO_6 superstructures having these advantages, the high recombination of photogenerated electron–hole pairs can limit their application, which still needs to be further enhanced. However, the high recombination rate of photo-carriers often troubles homojunction semiconductors. As fabricating a heterojunction is a well-known effective way to suppress the high photo-carrier recombination rates, many materials have been coupled with Bi_2WO_6, such as BiOBr [15], $Bi_2O_2CO_3$ [16], CdS [17], Co_3O_4 [18], WO_3 [19, 20] or $ZnFe_2O_4$ [21]. The results indicate that coupling with other materials can enhance the photocatalytic activity of pure Bi_2WO_6. Among these, WO_3 with a small bandgap (2.4–2.8 eV) can match well with Bi_2WO_6. More importantly, WO_3 is an inexpensive and promising material and is reported to have good photocatalytic performance. Gui and Zhang have prepared the WO_3/Bi_2WO_6 heterojunction which consisted of Bi_2WO_6 nanoplatelets decorated with WO_3 nanoparticles [19]; the advantage of the 3D flower-like structure of Bi_2WO_6, and the large specific surface area, could not survive in their samples.

In the work reported in this Letter, we have successfully prepared the flower-like WO_3/Bi_2WO_6 heterojunction by a facile hydrothermal method with heat treatment. The experimental results show that the flower-like WO_3/Bi_2WO_6 heterojunction has much greater applications for the photocatalytic degradation of Rhodamine B (RhB) under visible light irradiation than pure Bi_2WO_6 does. Moreover, a plausible mechanism of WO_3/Bi_2WO_6 on the degradation of RhB is discussed and confirmed by photocurrent and PL spectra.

2. Experimental

2.1. Preparation of WO_3/Bi_2WO_6 photocatalysts: All chemicals are reagent grade and used without further purification. Bi_2WO_6 was prepared by the hydrothermal method. Typically, 5.0 mmol $Bi(NO_3)_3{\cdot}5H_2O$ and 2.5 mmol $Na_2WO_4{\cdot}2H_2O$ was dissolved in 30 mL H_2O aqueous solution with strong magnetic stirring for 10 min. Subsequently, the $Na_2WO_4{\cdot}2H_2O$ aqueous solution was added dropwise into the $Bi(NO_3)_3{\cdot}5H_2O$ suspension. After stirring for 30 min, the obtained white suspension was transferred into a 100 mL Teflon-lined autoclave and heated at 180°C for 12 h, then cooled to room temperature naturally. The white precipitate was collected and washed with distilled water and ethanol several times, then dried under vacuum at 60°C for 10 h.

The synthesis process of WO_3/Bi_2WO_6 samples was as follows: an appropriate amount of $Na_2WO_4{\cdot}2H_2O$ was dissolved in 60 mL H_2O aqueous solution under stirring for 30 min. The as-prepared Bi_2WO_6 powder (2.5 mmol) was added into the above solution and stirred for 30 min, then the pH value of the suspension was adjusted to 1 by adding dropwise 4 mol/L HNO_3 solution. After stirring for 1 h, the light yellow precipitate was collected and washed with distilled water several times, then dried under vacuum at 60°C for 10 h. The WO_3/Bi_2WO_6 powder was obtained after calcination at 550°C for 4 h. The WO_3-modified Bi_2WO_6 powders with different mass ratios from 5 to 30% and pure WO_3 powder were prepared by following a similar procedure.

2.2. Characterisation: The crystal structure of the samples were investigated using X-ray diffraction (XRD, Model no: D/max2200pc, Japan) with Cu K_α radiation ($\lambda = 1.54$ Å) over the range of $10° \leq 2\theta \leq 70°$. The morphology and microstructure of the samples were obtained by a field-emission scanning electron microscope (FE-SEM, Model no: Hitachi S-4800). Diffuse-reflection absorption spectra of the samples were recorded on a Shimadzu UV-2550 spectrophotometer. The photoluminescence (PL) measurements were carried out on a Hitachi F-4500 fluorescence spectrophotometer. The photocurrent was conducted using an electrochemical workstation (Model no:

doi: 10.1049/mnl.2015.0147

CH1660D, CH Instruments, Shanghai). A three-electrode system was employed using a silver chloride electrode (Ag/AgCl) as a reference electrode, Pt wire as the counter electrode and the prepared samples as the working electrodes, 1 M Na_2SO_4 as the electrolyte, and a 300 W Xe lamp (wavelength range, distance between sample and lamp) was used as the light source. All measurements were carried out at room temperature.

2.3. Photocatalytic activity: The photocatalytic activities of the samples were evaluated via photocatalytic degradation of RhB in an aqueous solution under visible light irradiation. A 500 W Xe lamp with a 420 nm cutoff filter was used as the light source to provide visible light irradiation. In each experiment, 10 mg the sample was added into 10 mL of RhB aqueous solution with a concentration of 5 mg/L. When the light was turned on, 5 ml of the suspension was taken at given time intervals and separated the tiny photocatalyst particles by centrifugation. The RhB concentrations were detected using the absorption spectra.

3. Results and discussion

3.1. Crystal structures: XRD was used to investigate the phase structure of the samples. Fig. 1 shows the XRD patterns of the pure Bi_2WO_6 and WO_3/Bi_2WO_6 samples with different contents of WO_3. All the diffraction peaks of the pure Bi_2WO_6 are orthorhombic (JCPDS No. 39-0256); five diffraction peaks at $2\theta = 28.1°$, 32.5°, 46.4°, 56.7° and 58.3° are indexed to the (113), (200) (020), (026) (220), (313) and (226) directions, respectively [22]. In the WO_3/Bi_2WO_6 samples, the XRD patterns consist of diffraction peaks of orthorhombic Bi_2WO_6 and monoclinic WO_3 (JCPDS No. 2-1465). On the right side of the enlarged Fig. 1*b* we can clearly see the diffraction peaks of WO_3. The strongest peak of WO_3 is attributed to the (002), (020), (200) planes [23]. At the same time, with the increase of WO_3 content, the intensity of the WO_3 diffraction peaks and the crystallinity gradually increase. No impurity peak is found in the WO_3/Bi_2WO_6 composites. This suggests that the heterojunction photocatalyst is only composed of orthorhombic Bi_2WO_6 and monoclinic WO_3.

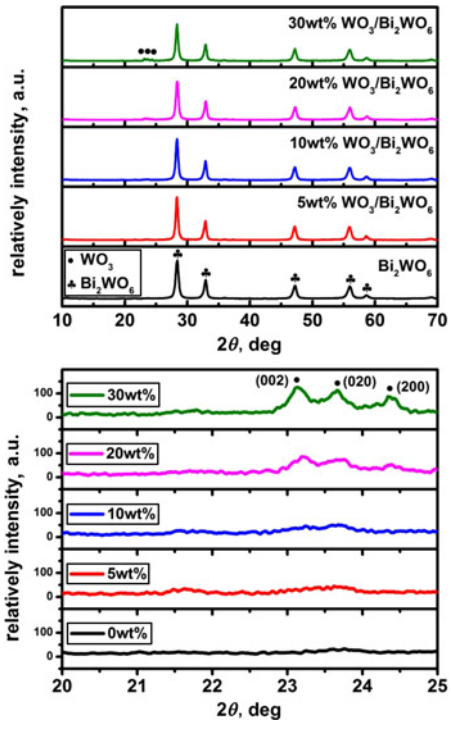

Figure 1 *XRD patterns of Bi_2WO_6 and WO_3/Bi_2WO_6 composite photocatalysts*

3.2. Morphology characterisation: The morphology and microstructure of the 10% WO_3/Bi_2WO_6 sample were investigated by SEM. Fig. 2*a* shows the panoramic morphology, which consists of spherical particles with diameters of about 4 μm. All the spherical particles are well dispersed. Figs. 2*b* and *c* show the image of an individual particle with high magnification, which reveals more detailed structural characteristics of the heterojunction photocatalysts. We can see that the spherical particle is flower-like and consists of 2D thin nanosheets with a thickness of about 40 nm. Many WO_3 nanoparticles are tightly attached to the nanoplates. Fig. 2*d* is the SEM image of the pure WO_3 sample, which is made up of small cubic particles of about 100 nm, but the particles aggregate because of sintering between small particles. We can obtain the more in-depth information of the 10% WO_3/Bi_2WO_6 sample by observing the TEM images of the samples. From Fig. 2*e*, which is the TEM image of the sample, we can see that some cubic particles are on the surface of the flower-like Bi_2WO_6. Fig. 2*f* is the HRTEM image of the sample. By carefully measuring the lattice parameters with a Digital Micrograph and comparing them with the data in JCPDS, two different kinds of lattice fringes are clearly observed. The lattice spaces of the Bi_2WO_6 crystallites are determined as 0.195 nm, belonging to the (220) crystallographic planes of orthorhombic Bi_2WO_6 (JCPDS No. 39-0256). The lattice space of the WO_3 crystallite is recognised as 0.332 nm, belonging to the (120) plane of the monoclinic WO_3 (JCPDS No. 72-1465), so the different heterojunction consists of flower-like Bi_2WO_6 and WO_3 cubic particles.

Fig. 3 is an SEM micrograph of the different samples (as described in the subcaptions). All the samples exhibit flower-like spherical particles which consist of nanosheets. The morphologies of the WO_3/Bi_2WO_6 samples are similar to that of the pure Bi_2WO_6, which indicates that the microstructures of the composite

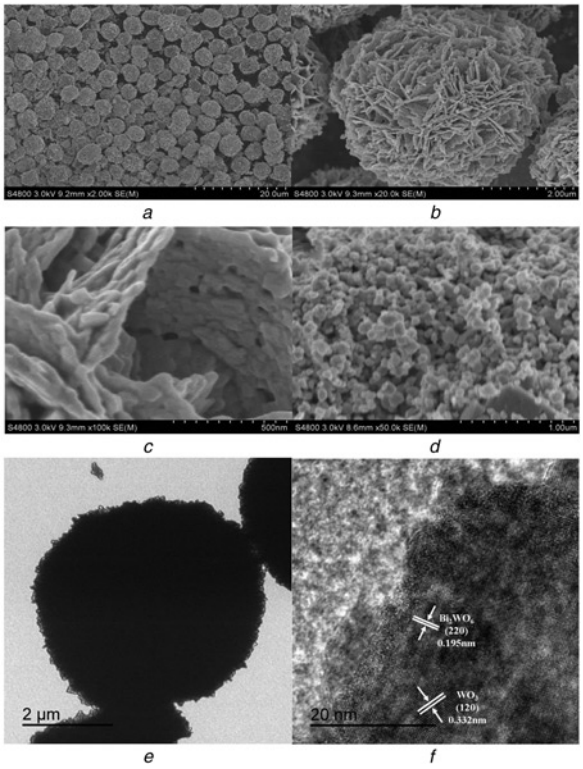

Figure 2 *SEM images*
a Overall morphology
b and *c* Detailed view of the 10% WO_3/Bi_2WO_6 on an individual sphere
d Pure WO_3
e and *f* TEM and HRTEM images of 10% WO_3/Bi_2WO_6

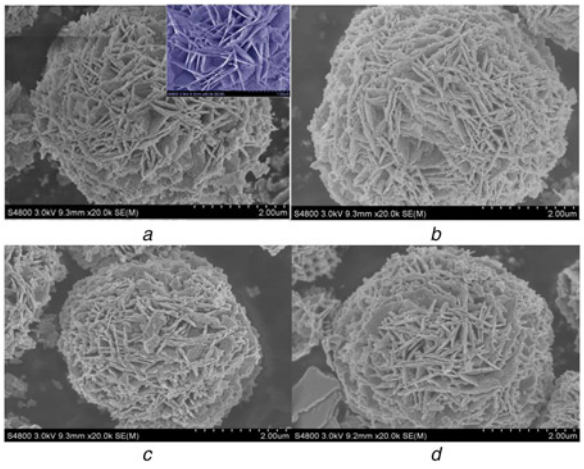

Figure 3 *SEM micrographs of the samples*
a Pure Bi_2WO_6
b 5% WO_3/Bi_2WO_6
c 20% WO_3/Bi_2WO_6
d 30% WO_3/Bi_2WO_6

samples have no change after the introduction of WO_3. As seen from the inset image in Fig. 3*a*, the nanoplates of Bi_2WO_6 are relatively smooth, and the thickness is about 27 nm.

3.3. Photocatalytic activity: The photocatalytic activity of the as-prepared samples was carried out using RhB as the model pollutant. Fig. 4*a* shows the temporal absorption spectra of RhB in the presence of 10% WO_3/Bi_2WO_6 under visible light irradiation ($\lambda > 420$ nm). During the photodegradation process, the intensity of the maximum absorption peak at about 553 nm decreases gradually. Meanwhile, the colour of the suspension fades gradually from pink to light green after irradiation for 150 min. Fig. 4*b* shows the photocatalytic degradation efficiency of different samples under visible light irradiation. It is clearly observed that all samples with WO_3 show higher photocatalytic activity than pure Bi_2WO_6 does. The 10% WO_3/Bi_2WO_6 shows the highest photocatalytic activity and has a 78.1% degradation ratio in 150 min under the same condition. As the WO_3 concentration further increases, the photocatalytic activity decreases. So the content of WO_3 has a great influence on the photocatalytic property of the WO_3/Bi_2WO_6 photocatalyst.

The stability and reusability of photocatalysts are very important for practical applications. As shown in Fig. 4*c*, the circulating runs were checked to evaluate the stability and reusability of the 10% WO_3/Bi_2WO_6 sample in the photodegradation of RhB under visible light. After every 150 min of photodegradation, the separated photocatalysts were washed with deionised water and dried to remove the ions absorbing on the surface after every reaction. From the results obtained, the photodecomposition rate of RhB still remains at about 78% after four cycling runs, which indicates that the composite photocatalyst is stable and reusable in the photocatalytic process.

3.4. Photocatalytic mechanisms: To better understand the improved photocatalytic property of the WO_3/Bi_2WO_6 heterojunction, we propose a plausible mechanism for the degradation of RhB. As shown in Fig. 5, the energy bandgap of Bi_2WO_6 and WO_3 is 2.7 eV ($E_{CB} = 0.24$, $E_{VB} = 2.94$ eV) [23] and 2.62 eV ($E_{CB} = 0.4$, $E_{VB} = 3.2$ eV) [24–26], respectively. The bandgaps of the two semiconductors match well with each other. According to the previous reports, the well-matched overlapping band structure in the composite could accelerate the separation of electrons and holes, and then improve the photocatalytic activity [27, 28]. Under visible light irradiation, both Bi_2WO_6 and WO_3 are excited synchronously and electron–hole pairs are produced. The Bi_2WO_6 acts as an electron-accepting semiconductor because of being less negative than WO_3. Photogenerated electrons easily transfer from the conduction band (CB) of WO_3 to that of Bi_2WO_6. At the same time, holes flow from the valence band (VB) of Bi_2WO_6 to that of WO_3. Thus, the photogenerated electrons and holes could be separated effectively, which is confirmed by the following transient photocurrent responses and PL spectra.

3.5. Transient photocurrent analysis: It is widely known that measuring transient photocurrent can gain an insight into the separation efficiency of the photogenerated electrons and holes. Fig. 6 displays the photocurrent–time (*I*–*t*) curves of the pure Bi_2WO_6 and WO_3/Bi_2WO_6 samples with typical on–off cycles of intermittent visible light irradiation. The photocurrent is drastically boosted once the light is turned on and returns quickly

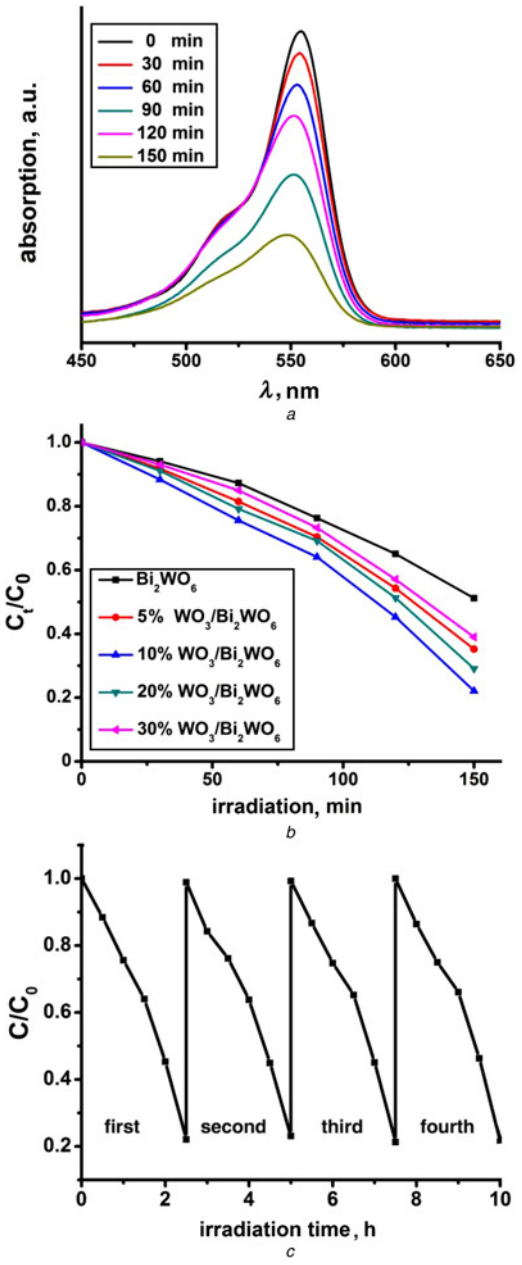

Figure 4 *Temporal UV–vis absorption spectra of RhB in the presence of 10% WO_3/Bi_2WO_6 under visible light irradiation (Fig. 4a); photocatalytic degradation curves (Fig. 4b); cycling runs for the degradation of RhB in the presence of 10% WO_3/Bi_2WO_6 under visible light irradiation (Fig. 4c)*

doi: 10.1049/mnl.2015.0147

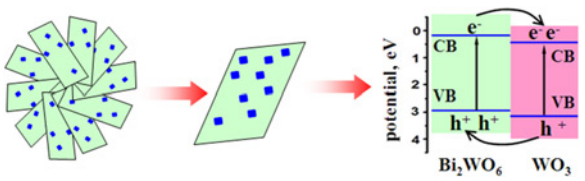

Figure 5 *Photocatalytic mechanism of WO_3/Bi_2WO_6 samples*

to its original value when the light is turned off. This indicates that the photocurrent arises from the illumination of light on the photo-anode. The initial current is due to the separation of electron–hole pairs at the semiconductor/electrolyte interface; holes are trapped by the reduced species in the electrolyte, while electrons are transported to the back contact substrate [29]. The results show that the photocurrent of the 10% WO_3/Bi_2WO_6 electrodes is significantly higher than that of the pure Bi_2WO_6 and other WO_3/Bi_2WO_6 samples, which indicates that the heterojunction has improved the separation of electron–hole pairs and inhibited the rapid recombination of photo-charges.

3.6. PL spectra analysis: The photocatalytic efficiency mainly depends on the recombination rate or lifetime of the photogenerated electron–hole pairs. To further investigate the separation efficiency of the electron–hole pairs, the PL spectra were used for examining the Bi_2WO_6 and WO_3/Bi_2WO_6 samples with an excitation wavelength of 300 nm. As shown in Fig. 7, all samples show an apparent characteristic emission peak from 420 to 480 nm and the strongest emitting peak at 458 nm is attributed to the intrinsic luminescence of Bi_2WO_6, which originates from the charge-transfer transitions between the hybrid orbital of Bi_{6s} and O_{2p} (VB) to the empty W_{5d} orbital (CB) in the WO_6^{2-} complex [30, 31]. With the WO_3 content increasing, the fluorescence emission peak position does not change. Compared with pure Bi_2WO_6, the WO_3/Bi_2WO_6 samples show a weaker PL intensity and the 10% WO_3/Bi_2WO_6 sample shows the weakest emission peaks. A weaker intensity of the peak represents a lower recombination probability of free charges. So an appropriate content of WO_3 in the composite sample is beneficial to separate the photogenerated electron–hole pairs and to increase the lifetime of the electron–hole pairs, and then to enhance the photocatalytic activity of Bi_2WO_6. This result agrees well with the photocatalytic activity and photocurrent analysis.

4. Conclusion: In summary, flower-like WO_3/Bi_2WO_6 heterojunctions have been prepared by a facile hydrothermal process with heat treatment. The photocatalytic experimental results indicate that the WO_3/Bi_2WO_6 heterojunction has better

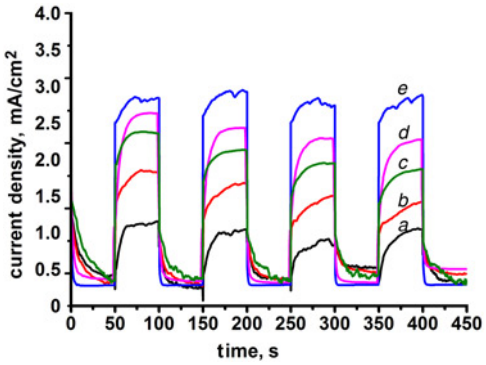

Figure 6 *Photocurrent transient responses of the samples*
a Pure Bi_2WO_6; *b* 5% WO_3/Bi_2WO_6; *c* 30% WO_3/Bi_2WO_6; *d* 20% WO_3/Bi_2WO_6; *e* 10% WO_3/Bi_2WO_6

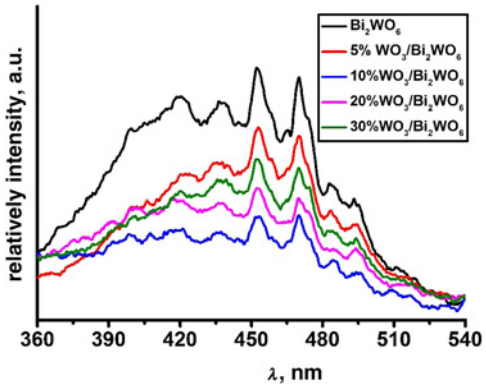

Figure 7 *PL spectra of Bi_2WO_6 and WO_3/Bi_2WO_6 samples*

photocatalytic activity than pure Bi_2WO_6. The doping content of WO_3 has great influence on the photocatalytic activity in the WO_3/Bi_2WO_6 heterojunction and the 10 wt% WO_3/Bi_2WO_6 composite exhibits the highest photocatalytic activity for the degradation of the RhB solution. The enhanced photocatalytic activity can be attributed to the effective separation and transfer of photogenerated electron–hole pairs. The mechanism has been discussed by energy band position and has been confirmed by photocurrent and PL spectra. The flower-like WO_3/Bi_2WO_6 heterojunction has good potential for the degradation of organic pollutants due to its good and stable photocatalytic activity.

5. Acknowledgements: The authors acknowledge financial support from the National Science Foundation of China (51272147), the Academic Backbone Cultivation Program of the Shaanxi University of Science & Technology (XSGP201203) and from the Graduate Innovation Fund of the Shaanxi University of Science and Technology.

6 References

[1] Chen C.C., Ma W.H., Zhao J.C.: 'Semiconductor-mediated photodegradation of pollutants under visible-light irradiation', *Chem. Soc. Rev.*, 2010, **39**, pp. 4206–4219
[2] Cui W.Q., An W.J., Liu L., Hu J.S., Liang Y.H.: 'Novel Cu_2O quantum dots coupled flower-like BiOBr for enhanced photocatalytic degradation of organic contaminant', *J. Hazard. Mater.*, 2014, **280**, pp. 417–427
[3] Guan M.L., Xiao C., Zhang J., *ET AL.*: 'Vacancy associates promoting solar-driven photocatalytic activity of ultrathin bismuth oxychloride nanosheets', *J. Am. Chem. Soc.*, 2013, **135**, pp. 10411–10417
[4] Ge L., Han C.C., Liu J.: 'Novel visible light-induced g-C_3N_4/Bi_2WO_6 composite photocatalysts for efficient degradation of methyl orange', *Appl. Catal. B, Environ.*, 2011, **108**, pp. 100–107
[5] Li J.Q., Liu Z.X., Wang D.F., Zhu Z.F.: 'Visible-light responsive carbon–anatase–hematite core–shell microspheres for methylene blue photodegradation', *Mater. Sci. Semicon. Proc.*, 2014, **27**, pp. 950–957
[6] Wu L., Yu J.C., Wang X.C., Zhang L.Z., Yu J.G.: 'Characterization of mesoporous nanocrystalline TiO_2 photocatalysts synthesized via a sol-solvothermal process at a low temperature', *J. Solid State Chem.*, 2005, **178**, pp. 321–328
[7] Zhang L., Zhu Y.F., He Y., Li W., Sun H.B.: 'Preparation and performances of mesoporous TiO_2 film photocatalyst supported on stainless steel', *Appl. Catal. B, Environ.*, 2003, **40**, pp. 287–292
[8] Ge L., Xu M.X., Fang H.B.: 'Photo-catalytic degradation of methyl orange and formaldehyde by Ag/$InVO_4$ – TiO_2 thin films under visible-light irradiation', *J. Mol. Catal. A, Chem.*, 2006, **258**, pp. 68–76
[9] Li J.Q., Wang D.F., Guo Z.Y., Zhu Z.F.: 'Preparation, characterization and visible-light-driven photocatalytic activity of Fe-incorporated TiO_2 microspheres photocatalysts', *Appl. Surf. Sci.*, 2012, **263**, pp. 382–388
[10] Feng N.D., Wang Q., Zheng A.M., *ET AL.*: 'Understanding the high photocatalytic activity of (B, Ag)-codoped TiO_2 under solar-light

irradiation with XPS, solid-state NMR, and DFT calculations', *J. Am. Chem. Soc.*, 2013, **135**, pp. 1607–1616
[11] Zhang Z.J., Wang W.Z., Yin W.Z., Shang M., Wang L., Sun S.M.: 'Inducing photocatalysis by visible light beyond the absorption edge: effect of up conversion agent on the photocatalytic activity of Bi_2WO_6', *Appl. Catal. B, Environ.*, 2010, **101**, pp. 68–73
[12] Wang X.J., Chang L.L., Wang J.R., Song N.N., Liu H.L., Wan X.L.: 'Facile hydrothermal synthesis of Bi_2WO_6 microdiscs with enhanced photocatalytic activity', *Appl. Surf. Sci.*, 2013, **270**, pp. 685–689
[13] Zhang N., Ciriminna R., Pagliaro M., Xu Y.J.: 'Nanochemistry-derived Bi_2WO_6 nanostructures: towards production of sustainable chemicals and fuels induced by visible light', *Chem. Soc. Rev.*, 2014, **43**, pp. 5276–5287
[14] Zhang L.S., Wang W.Z.: 'Fabrication of flower-like Bi_2WO_6 superstructures as high performance visible-light driven photocatalysts', *J. Mater. Chem.*, 2007, **17**, pp. 2526–2532
[15] Xia J.X., Di J., Yin S., *ET AL.*: 'Facile fabrication of the visible-light-driven Bi_2WO_6/BiOBr composite with enhanced photocatalytic activity', *RSC Adv.*, 2014, **4**, pp. 82–90
[16] Huang X.W., Chen H.F.: 'One-pot hydrothermal synthesis of $Bi_2O_2CO_3/Bi_2WO_6$ visible light photocatalyst with enhanced photocatalytic activity', *Appl. Surf. Sci.*, 2013, **284**, pp. 843–848
[17] Ge L., Liu J.: 'Synthesis and photocatalytic performance of novel CdS quantum dots sensitized Bi_2WO_6 photocatalysts', *Mater. Lett.*, 2011, **65**, pp. 1828–1831
[18] Xiao Q., Zhang J., Xiao C., Tan X.K.: 'Photocatalytic degradation of methylene blue over Co_3O_4/Bi_2WO_6 composite under visible light irradiation', *Catal. Commun.*, 2008, **9**, pp. 1247–1253
[19] Gui M.S., Zhang W.D.: 'One-step hydrothermal preparation strategy for nanostructured WO_3/Bi_2WO_6 heterojunction with high visible light photocatalytic activity', *Chem. Eng. J.*, 2012, **197**, pp. 283–288
[20] He G.H., He G.L.: 'Synthesis and visible light photocatalytic behavior of WO_3 (core)/Bi_2WO_6 (shell)', *J. Mol. Catal. A, Chem.*, 2014, **385**, pp. 106–111
[21] Li J.Q., Liu Z.X., Zhu Z.F.: 'Magnetically separable ternary hybrid of $ZnFe_2O_4$-Fe_2O_3-Bi_2WO_6 hollow nanospheres with enhanced visible photocatalytic property', *Appl. Surf. Sci.*, 2014, **320**, pp. 146–153
[22] Zhang L.S., Wang W.Z., Zhou L., Xu H.L.: 'Bi_2WO_6 nano- and microstructures: shape control and associated visible-light-driven photocatalytic activities', *Small*, 2007, **9**, pp. 1618–1625
[23] Ge L., Liu J.: 'Efficient visible light-induced photocatalytic degradation of methyl orange by QDs sensitized CdS-Bi_2WO_6', *Appl. Catal. B, Environ.*, 2011, **105**, pp. 289–297
[24] Adhikari S., Sarkar D., MaitiS H.S.: 'Synthesis and characterization of WO_3 spherical nanoparticles and nanorods', *Mater. Res. Bull.*, 2014, **49**, pp. 325–330
[25] Kwong W.L., Savvides N., Sorrell C.C.: 'Electrodeposited nanostructured WO_3 thin films for photoelectrochemical applications', *Electrochim. Acta*, 2012, **75**, pp. 371–380
[26] Ng C., Iwase A., Ng Y.H., Amal R.: 'Transforming anodized WO_3 films into visible-light-active Bi_2WO_6 photoelectrodes by hydrothermal treatment', *J. Phys. Chem. Lett.*, 2012, **3**, pp. 913–918
[27] Cui W.Q., An W.J., Liu L., Hu J.S., Liang Y.H.: 'Synthesis of CdS/BiOBr composite and its enhanced photocatalytic degradation for Rhodamine B', *Appl. Surf. Sci.*, 2014, **319**, pp. 298–305
[28] Yu C.L., Li G., Kumar S., Yang K., Jin R.C.: 'Phase transformation synthesis of novel Ag_2O/Ag_2CO_3 heterostructures with high visible light efficiency in photocatalytic degradation of pollutants', *Adv. Mater.*, 2014, **26**, pp. 892–898
[29] Tian B.Z., Dong R.F., Zhang J.M., Bao S.Y., Yang F., Zhang J.L.: 'Sandwich-structured AgCl@Ag@TiO_2 with excellent visible-light photocatalytic activity for organic pollutant degradation and *E. coli* K12 inactivation', *Appl. Catal. B, Environ.*, 2014, **158–159**, pp. 76–84
[30] Li J.Q., Guo Z.Y., Zhu Z.F.: 'Ag/Bi_2WO_6 plasmonic composites with enhanced visible photocatalytic activity', *Ceram. Int.*, 2014, **40**, pp. 6495–6501
[31] Xiao Q., Zhang J., Xiao C., Tan X.K.: 'Photocatalytic degradation of methylene blue over Co_3O_4/Bi_2WO_6 composite under visible light irradiation', *Catal. Commun.*, 2008, **9**, pp. 1247–1253

doi: 10.1049/mnl.2015.0147